

Multimodal Brain-Computer Interface for In-Vehicle Driver Cognitive Load Measurement: Dataset and Baselines

Prithila Angkan, Behnam Behinaein, Zunayed Mahmud, Anubhav Bhatti, Dirk Rodenburg, Paul Hungler, Ali Etemad, *Senior Member, IEEE*



Abstract—Through this paper, we introduce a novel driver cognitive load assessment dataset, CL-Drive, which contains Electroencephalogram (EEG) signals along with other physiological signals such as Electrocardiography (ECG) and Electrodermal Activity (EDA) as well as eye tracking data. The data was collected from 21 subjects while driving in an immersive vehicle simulator, in various driving conditions, to induce different levels of cognitive load in the subjects. The tasks consisted of 9 complexity levels for 3 minutes each. Each driver reported their subjective cognitive load every 10 seconds throughout the experiment. The dataset contains the subjective cognitive load recorded as ground truth. In this paper, we also provide benchmark classification results for different machine learning and deep learning models for both binary and ternary label distributions. We followed 2 evaluation criteria namely 10-fold and leave-one-subject-out (LOSO). We have trained our models on both hand-crafted features as well as on raw data.

Index Terms—Driver, cognitive load, wearables, brain-computer interfaces, deep learning.

1 INTRODUCTION

A large number of accidents and collisions occur on the roads every year. While many of these accidents are caused by distracted drivers, for instance due to distraction or drowsiness [1]. Distraction, meanwhile, can be caused by a number of personal or ambient factors, including high cognitive load due to engagement with secondary tasks [2], [3], [4]. Cognitive load refers to the quantity of information our working memory can process at a given time. In other words, it is the amount of cognitive resources required to accomplish a task. In general, two categories of cognitive load, intrinsic and extraneous, have been described in the literature [5]. While intrinsic cognitive load is defined as the inherent complexity of a given task, extraneous cognitive load refers to the cognitive resources demanded by environmental factors that are task-irrelevant [5]. The success or failure in performance toward a particular task, on the other hand, is influenced by the amount of cognitive load experienced by the person performing the task [6]. If the cognitive load increases beyond a certain point, the individual’s performance will degrade, which in case of driving may increase the likelihood of road accidents.

In order to reduce the number of road accidents caused by high cognitive load, recent intelligent technologies inte-

grated into vehicles should possess the ability to measure cognitive load and alarm the user should dangerously high amounts of it be detected. Brain-computer interfaces (BCI) have recently gained traction in providing advanced means of communication between humans and machines. In particular, head-worn Electroencephalogram (EEG) devices allow for non-invasive yet accurate human-machine interactions. To this end, machine learning and deep learning techniques can be used to learn from datasets with various types of driver-related signals (including EEG). Additionally, these datasets require quantitative cognitive load scores to be measured and provided at frequent intervals, so that they could be used to train the machine learning models. While a number of relevant datasets have been collected and published in recent years [7], [8], [9], [10], [11], a number of problems persist. First, while a number of datasets for cognitive load do exist, they have often been captured in non-vehicle scenarios. In fact, to our knowledge, only [7] has studied cognitive load in the context of driving. Third, while most existing datasets on cognitive load are in fact ‘multimodal’, the notion of BCI with auxiliary wearable signals has not been widely explored [7], [8], [9], [10], [11]. Lastly, in most existing works in the area, the focus has been solely on cognitive load or distraction caused by task-irrelevant activities, overlooking the fact that performing the main task itself (in our case, driving) can be a strong source of high cognitive load.

In this paper, we introduce a novel driver cognitive load assessment dataset containing EEG signals along with other physiological signals such as Electrocardiography (ECG) and Electrodermal Activity (EDA) as well as eye tracking data. This dataset, which we name CL-Drive, is collected from 21 subjects while driving in an immersive vehicle simulator in diverse situations capable of inducing various levels of cognitive load in the subjects. Each subject performs driving tasks in 9 complexity levels for 3 minutes each and reports their subjective cognitive load every 10 seconds throughout the experiment as ground-truth cognitive load labels. In this paper, we also provide benchmark classification results for different machine learning and deep learning models. Both raw signals as well as popular features supported by the literature have been used as inputs. We follow

two important evaluation criteria, namely 10-fold and leave-one-subject-out (LOSO). Our benchmarking demonstrates that cognitive load induced by driving can be measured with reasonable accuracy using EEG and auxiliary wearable signals.

Our contributions in this paper are summarized as follows:

- We collect a dataset, CL-Drive, that can allow researchers to evaluate driving-induced cognitive load, which can be useful for developing automated alarm systems for intelligent vehicles.
- CL-Drive provides data from various modalities including EEG, ECG, EDA and Gaze, which is a rich source for training machine learning systems capable of performing cognitive load assessment.
- CL-Drive contains dense and frequent subjective ratings which are spread only 10 seconds, allowing for more reliable and frequent automated cognitive load measurement by learned models.

The rest of this paper is summarized as follows. In Section 2, we first provide a study of cognitive load followed by an overview of the publicly available cognitive load datasets that contain physiological signals. Section 3 explains the experimental setup, including sensor configurations, driving simulator details, cognitive load assessment, and data collection protocol. Next, we discuss the data preprocessing, feature extraction, normalization, and baseline classifiers in section 4. Lastly, in Section 5 we provide the results and discussions.

2 RELATED WORK

2.1 Cognitive Load Measurement

Prior research has shown that measuring cognitive load from physiological signals [12], [13] continues to be a challenging task [14], [15]. There are both subjective and objective measures that are commonly used to evaluate cognitive load levels that involve: (i) self-reporting, (ii) dual-task measures, and (iii) physiological measures [16]. The PAAS scale [17], shown in Table 1 is most commonly used for self-reported subjective cognitive load labels. The National Aeronautics and Space Association Task Load Index (NASA-TLX) [18] is also commonly used as a self-reporting tool. Dual-task measurement involves the individual performing two tasks at the same time. One way of designing this is to measure knowledge gain from one task and response time for the other task [19]. In [20], another way of implementing dual-task measurement was explored, which was by performing a continuous secondary task while learning the primary task. There are several physiological parameters that have also been used as cognitive load measures in the past. This includes variation in pupil diameter and blink rate [21], [22], heart rate variability [23], and electrocardiogram (ECG) [24] to name a few.

2.2 Cognitive Load in Driving

In the area of driving, prior works have studied cognitive load mainly in the context of the driver being engaged by secondary tasks such as using mobile phones or performing

TABLE 1: PAAS subjective cognitive load scores used in this study.

PAAS Subjective Cognitive Load Scores	Description
1	Very, very low
2	Very low
3	Low
4	Rather low
5	Neither low nor high
6	High
7	Rather high
8	Very high
9	Very, very high

some other in-vehicle activities [2], [25], [26], [3], [27]. In [2], the cognitive load of drivers was measured when the drivers were involved in verbal conversation and word games while driving. As a result, the cognitive load induced was due to the combination of both primary as well as secondary tasks. A remote eye tracker was used to measure the pupil size of all 32 participants which in turn was used to estimate the cognitive load of the participants. The ground truth was the performance measures which they calculated using lane position and degree of rotation of the steering wheel, and subsequently evaluated the relationship between the change in pupil diameter and driving performance.

Driving performance while interacting with an iPod¹ was evaluated in [25]. It was observed during a multi-session setup, that the cognitive load of the participants during the first sessions was higher, hence the driving performance (e.g., perception response time (PRT) while braking and overall control of the vehicle), was lower in comparison to the later sessions. The experiment was carried out on 19 participants using simulated vehicle. Next, in [26], the high cognitive load of drivers was evaluated using EEG signals in 3 different driving conditions, namely: no secondary task (baseline), low cognitive load task, and high cognitive load task. The low and high cognitive load tasks were based on N-back tasks used in [28], [29]. GSR, eye tracking, respiration rate (RR), and accelerator release time (ART) data were collected during the experiments. The data was collected from 37 participants in a vehicle simulator. The NASA-TLX was used to collect the participants subjective rating at the end of the experiment. In [3], the cognitive load of participants was evaluated using eye video data extracted from facial videos during driving. Three different N-back tasks were used as secondary tasks, which were also used to quantify the ground truth levels. Hidden Markov models and 3D-CNN were then used to evaluate the result. In another paper [27], the cognitive load of participants was evaluated while driving and performing a 1-back task. EEG data was collected from 36 participants. To evaluate the performance, case-based reasoning classifiers were used [30]. A few other prior works such as [2], [25], [26] have used more simple approaches based on predefined metrics (e.g., required time to break, degree of motion of the steering wheel, etc.) to measure cognitive load from physiological signals.

Besides cognitive load, other factors such as driver emotions [31], [32], [33] and vigilance [34], [35], [36], have been

1. <https://www.apple.com/ca/>

TABLE 2: Existing datasets in the literature that study cognitive load using physiological signals.

Dataset	Year	Sub.	Mental State	Modalities	Stimuli
Driver Workload [7]	2013	10	Mental workload of the driver	ECG, BTemp, SCR	Watching driving videos, Driving in real environment
MMOD-COG [8]	2019	40	Cognitive load	ECG, EDA, Speech	Arithmetic, Reading
CLAS [9]	2019	62	Cognitive Load, negative emotion and mental stress	ECG, PPG and EDA	Math problems, Logic problems and Stroop test
CogLoad [10]	2020	23	Cognitive load, Personality traits	heart rate, beat to beat interval, EDA, ST, and ACC	Different cognitive load tasks (2-back and 3-back tasks, visual cue task etc.)
Snake [10]	2020	23	Cognitive load	heart rate, beat to beat interval, EDA, ST, and ACC	Snake game on a smartphone
Kalatzis et al. [11]	2021	26	Cognitive load	ECG, RR	MATB-II

widely studies in the literature. While these works may maintain some similarities to works on cognitive load, they are in fact different driver attributes which are outside the scope of this study. Moreover, the notions of affect and distraction have been more widely studied for drivers, as opposed to cognitive load which is a less explored area.

2.3 BCI

BCI systems can communicate the neural activities in the brain directly with an external device [6], [37]. Research has shown that BCI can play a vital role in interpreting the cognitive load induced while driving [6], [37]. This is due to the fact that the fronto-parietal brain regions along with sub-cortical regions can be engaged while experiencing varying amounts of cognitive load [38]. EEG, is a non-invasive method which measures the potential difference caused by the electrical activity in the brain [39], [40]. This property of EEG allows it to capture changes in brain activity while experiencing variations in cognitive load, which makes it a very good candidate for cognitive load evaluation. Multimodal approaches have proven effective at magnifying the accuracy of cognitive load assessment in the past [41]. Apart from EEG, research has shown that both the sympathetic nervous system (SNS) which controls the skin conductance response and automatic nervous system which controls the heart rate variability (HRV) are impacted by cognitive load [42], [43], [44]. Prior research has also shown significant correlation between changes in pupil size, blink rate, saccade, and fixation with cognitive load [45], [46].

2.4 Public Cognitive Load Datasets

Previous research has examined the induction of cognitive load in drivers with a subsequent evaluation of driving performance under varying cognitive load levels [47], [48]. Some other publications have studied cognitive load under a variety of different experimental setups [49], [24]. There is evidence that affect and cognitive load are interrelated and affect has a significant impact on cognitive load [50]. Though a wide range of studies have been done to study the impact of affect on EEG [51], [52], the available datasets for cognitive load are indeed quite limited. In this section, we provide an overview of the publicly available datasets for cognitive load with physiological signals. Table 2 presents a summary of these datasets.

The Driver Workload dataset [7], provides multimodal data to evaluate driver workload using ECG, body temperature, and skin conductance response (SCR). The dataset was collected from 10 participants with the goal of evaluating cognitive load of drivers on different types of roads and in different driving environments. In addition to the physiological signals, two cameras were also used to record the driving route as well as the participant’s facial videos. The video data were not made public for privacy purposes. The data was collected as the participants drove the car for 30 minutes. Participants subjective ratings were collected by watching videos of their own driving at the end of the activity.

The MMOD-COG [8] dataset was recorded from 40 different subjects for cognitive load assessment during reading and arithmetic tasks. ECG and EDA were recorded from the subjects in addition to speech. The experiment was divided into reading and arithmetic segments where in the reading segment, two separate digits were shown for 5 seconds and repeated with different digits 20 times. The arithmetic segment was divided into high and low cognitive load levels and a total of 40 problems were asked to be solved by each participant. The CLAS dataset [9] was collected from 62 participants and was obtained by recording various cognitive load levels induced by tasks such as mathematics and logic problems as well as the Stroop test [53]. In addition to cognitive load, audio-visual stimuli were used to induce emotional variations in the participants. Physiological data was collected using ECG, Plethysmography (PPG), EDA, and accelerometer (ACC) data. The next dataset, CogLoad [10] was also a multimodal dataset with 23 participants who performed 6 different computer tasks during the collection process. The physiological data collected was heart rate, beat to beat interval, EDA, skin temperature (ST), and ACC. The task was divided into two segments where the first segment involved understanding the participant’s degree of cognitive resources and their personality traits using two N-back tasks [10], [54]. Whereas, in the second segment, 6 different tasks that required varying levels of cognitive load were performed. In addition, in order to completely occupy the cognitive resources of the participants, a secondary task was also given to them to perform.

Another multimodal dataset consisting of heart rate, EDA, ST, and ACC was collected from 23 participants while they played the Snake game on a smartphone [10].

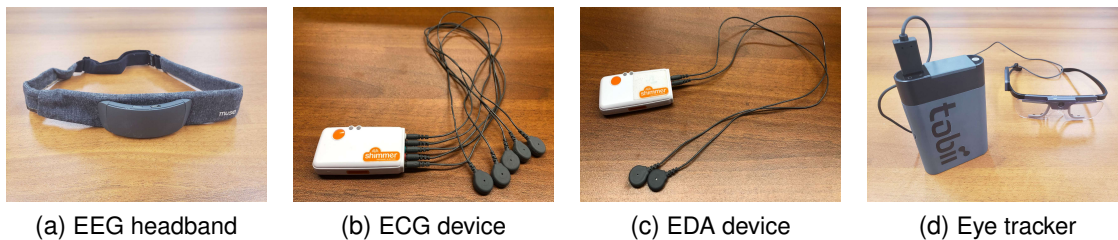


Fig. 1: Wearable EEG, ECG, EDA, and Gaze devices.

This dataset named Snake [10], was collected with varying cognitive load levels where the amount of cognitive load experienced by the participants was controlled by the changing speed of the game. The task consisted of 3 complexity levels, high, medium and low, which lasted 2 minutes each. After the task completion, the participants answered the NASA TLX [18] questionnaire along with two other 7-point Likert scale questions. Finally, Kalatzis et al. [11] presented a dataset that has been collected from 26 participants. In this dataset, the cognitive load of the participants was assessed using ECG and respiration rate (RR) data. High and low cognitive load data were collected as the participants used the MATB-II software [55] while the NASA TLX [18] questionnaire was used to collect ground truth values for the two cognitive load levels.

3 EXPERIMENT SETUP AND DATA COLLECTION

In this section, we discuss the experimental protocol used in the study. This includes specifics on the setup for the sensors and driving simulator as well as details of the participants, diving scenarios, and cognitive load assessment.

3.1 Sensors

During the experiments which will be described in Section 3.7, we use four different sensors to collect physiological signals from which to measure cognitive load. Following is a description of each sensor type, namely EEG, ECG, EDA, and Gaze, in detail. Figure 1 shows the sensors used in our study, while Figure 2 shows their detailed sensors placement.

EEG. For collecting EEG signals the Muse S² headband shown in Figure 1a is used. The device has 4 channels where 2 of them are frontal electrodes located at the forehead in locations AF7 and AF8 (according to the international 10-20 system [56], [57]) while the remaining 2 are temporal electrodes located behind the ears in locations TP9 and TP10. Figure 1a depicts the Muse EEG device while in Figure 2a, we present the sensor locations of this EEG headset. As shown in the figure, the reference electrode is located at the middle of the forehead in location FpZ. The sampling rate of the EEG headband is 256 Hz. Conductive gel is used to enhance the conductivity between the electrode and the skin.

ECG. ECG signals are collected through the Shimmer³ sensors [58], which is shown in Figure 1b. As depicted in Figure

2b, this wearable device uses 5 standard pre-gelled adhesive electrodes from the chest and abdominal area. Among the 4 electrodes, the Right Arm (RA) and Left Arm (LA) are placed on the left and right sides of the manubrium, while Right Leg (RL) and Left Leg (LL) are placed right above the lower costal margin. The reference electrode denoted by Vx is placed slightly on the right of the sternum. The signals collected are LL-RA, LA-RA, and Vx-RA at a sampling frequency of 512 Hz. The Shimmer is worn by the participants using a belt and a cradle.

EDA. Similar to ECG, the EDA signal is collected using a Shimmer wearable device [58] as shown in Figure 1c. The data is collected using 2 electrodes placed on the left side of the abdomen which is shown in Figure 2c. The sampling frequency of the EDA Shimmer device is 128 Hz

Gaze Figure 1d shows a Tobii device⁴ used to collect eye tracking data. The device is comprised of a head unit and a recording unit. Inside the device there are 2 cameras per eye as well as a wide angle scene camera. From the eye tracking device we record the specific eye movement events such as saccade, fixation, and others. The sampling frequency is 50 Hz. Figure 2d illustrates the placement of the eye tracking device along with the EEG headset.

3.2 Experiment Test-bed

In order to simulate driving and be able to control the parameters surrounding the driving experience, we use a driving simulator⁵ shown in Figure 3. The driving simulator includes elements similar to a real car, including steering wheel, dashboard, accelerator, and brake. These components combined with a motion system provides participants with a more realistic driving sensation. The motion system can emulate real-life motions up to 100 Hz in frequency. This includes vibrations from road texture, acceleration, braking, speeding, and turning along with other essential movements to provide users with engaging haptic feedback. Additionally, there are three 55 inch LCD screens which provide a 180 degree view from the front, plus two additional screens for the blind spots, together creating an immersive experience. Each front screen has a display resolution of 1920 × 1080 pixels. Moreover, directional sound is incorporated using a surround sound system. The sound is intended to mimic typical sounds heard while driving including the sound of the engine, speeding and passing vehicles, and horns, among others.

4. <https://www.tobii.com/product-listing/tobii-pro-glasses-2/>

5. <https://viragesimulation.com/vs500m-car-simulator-training-and-research/>

2. <https://choosemuse.com/muse-s/>

3. <https://shimmersensing.com/product/shimmer3-ecg-unit-2/>

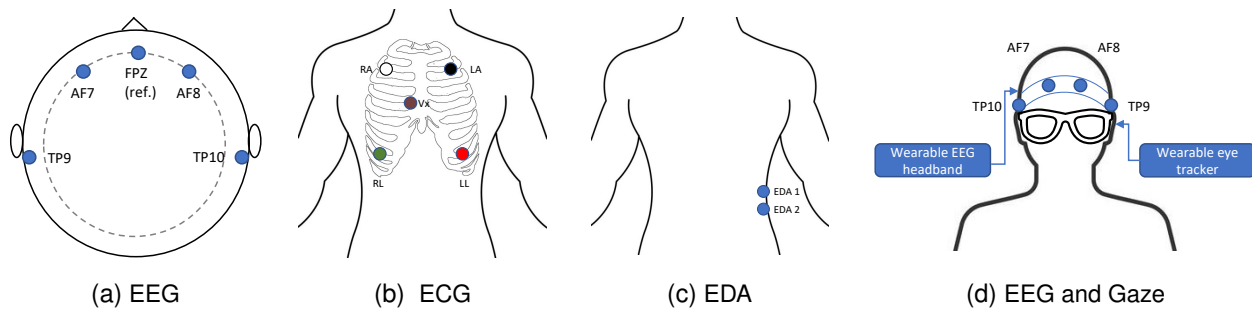


Fig. 2: EEG, ECG, EDA, and Gaze electrode placements.



Fig. 3: The immersive vehicle simulator used in this study.

A debrief station is designed to provide a complete video of the participant and simulation screens during the experiment along with performance graphs. There is a webcam mounted on the top of the middle frontal screen, which has a resolution of 720p. The camera records video of the participants while driving in the simulator. The performance information displayed in the debrief station includes driving performance data, including the time required for breaking and acceleration, possible crashes, and others. This data can also be used for performance analysis.

3.3 Driving Scenarios

The simulator comes with a number of pre-built driving scenarios in which the vehicle type, environmental conditions, and other factors can vary. Each scenario consists of a number of tasks that need to be performed, e.g., keeping a speed of above a certain threshold. Moreover, each scenario has a designated complexity level. We choose 9 different scenarios, one from each complexity level. The duration of each scenario is set to 3 minutes. An orientation scenario was designed and performed by each participant at the beginning of the session to allow the participant to adapt to the simulator. Table 3 shows the description of each driving scenario along with its corresponding complexity level.



Fig. 4: The experiment flow.

3.4 Simulation Adaptation Syndrome

It has been shown in prior research that Simulation Adaptation Syndrome (SAS) can affect different participants [59], [60]. SAS can range from feeling minor discomfort to severe symptoms such as dry mouth, dizziness, vertigo, vomiting, nausea, and disorientation while taking part in simulations such as driving a vehicle [61]. The main cause of SAS is the discrepancy between the sensory inputs such as visual and vestibular system (which is responsible for our sense of balance [62], [63]). One of the challenges we faced during our study was avoiding and minimizing SAS. As recommended in the simulator instructions, we followed the following 5 steps to manage and reduce SAS as much as possible:

- 1) **Cool room:** the simulator room must be cool and well ventilated;
- 2) **Confident introduction:** must create a calm and relaxed environment;
- 3) **Cautious alert:** moving on slowly to allow the driver's time to adjust;
- 4) **Careful observation:** must actively look for signs and symptoms of SAS;
- 5) **Cease driving:** must pause immediately on observing the slightest sign of SAS.

SAS can be managed by carefully monitoring the participant's level of discomfort using a Likert scale and asking the participants to do an intermittent self assessment. In our case, the participants were asked to self report on their SAS level every minute using a 9-point Likert scale as shown in Table 4, which was made based on the Motion Sickness Questionnaire (MSQ) [64], Simulator Sickness Questionnaire (SSQ) [65], and The Motion Sickness Assessment Questionnaire (MSAQ) [66]. Based on these pre-cautions and careful monitoring, SAS resulted in pausing and discontinuing only 2 participants.

TABLE 3: Driving scenario details

Scenario/ Complexity	Simulation	Description
0/Orientation	Highway driving	Maintain centre
1	Highway driving	80km/h
2	Night time driving	80km/h
3	Night time driving in the highway w/ snow	80km/h
4	Tennis ball challenge	Hit the tennis ball with the tire, maintain accuracy, try to accelerate
5	Slalom challenge	Navigate through gates, maintain accuracy, try to accelerate
6	Narrow passage challenge	Navigate through gates, maintain accuracy, try to accelerate
7	90-degree turn challenge	Take 90 degrees left and right turns, maintain accuracy, try to accelerate
8	3-point turn challenge	Drive while following instructions, take 3 point turn
9	Narrow alley challenge	Navigate through narrow alley, maintain accuracy, try to accelerate

TABLE 4: SAS levels and their corresponding description.

SAS Level	Description
1	Feeling no adverse effects
2	Feeling very mild discomfort
3	Feeling mild discomfort
4	Feeling mild to moderate discomfort
5	Feeling moderate discomfort
6	Feeling moderate to pronounced discomfort
7	Feeling pronounced discomfort
8	Feeling pronounced to severe discomfort
9	Feeling severe discomfort (potential for vomiting)

3.5 Participants

Data was collected from 23 participants including 17 females and 6 males. Prior to the simulation, participants were provided with detailed information on the experimental process and the research team received written consent. The study was approved by Queen’s University’s General Research Ethics Board (GREB). Among the 23 participants, 2 data collection sessions were stopped due to high levels of SAS, while the data from another 3 sessions was incomplete due to device or connectivity issues. Specifically, for participant 13, we only have data for scenarios 3, 4, 5, 6, and 9, while for participant 16, we have data for scenarios 1, 5, 6 and 9. Finally, for participant 18, we have the data for scenarios 1 to 6. While the data from the two sessions that were incomplete due to SAS are not incorporated in the dataset as they were interrupted too early in the process, the data from the three incomplete sessions are incorporated.

3.6 Cognitive Load Self-Assessment

Participant cognitive load self-assessment ratings were used as ground truth labels in this study. As shown in Table 1, PAAS subjective cognitive load scores consist of 9 levels [67]. A looping audio cue was generated every 10 seconds during the experiments to prompt the participants to verbally report their cognitive load, and a member of the research team recorded the reported scores. Figure 6 presents the distribution of the recorded output scores for all the participants.

3.7 Experiment Protocol

Participants were given clear descriptions about the data collection protocol and equipment. After careful sensor placement, participants were asked to sit in the driving seat of the simulator and the sensors were connected via Bluetooth to a data collection station. First, 3 minutes of

baseline data was collected from each participant which could be used for future normalization of the signals. To become adapted to the simulated driving environment and make sure that participants had a clear understanding about the ‘low’, ‘medium’, and ‘high’ complexity levels, and also to reduce the SAS level, participants were asked to perform the *Orientation* scenario mentioned earlier in Table 3. Following every 3-minute driving scenario (see Table 3), the participants were given a resting time of 2 minutes to allow them to rest, reduce the possibility of SAS, and come back to a relatively lower cognitive load state. Followed by the resting period, a 2-minute baseline was collected before each new scenario. The experiment flow is shown in Figure 4. During all these experiments, the wearable sensors discussed earlier in Section 3.1 were used to record the respective signals from the participants. Figure 5 we illustrate a sample from each captured modality in both high and low cognitive load scenarios.

4 DATA PROCESSING

In this section, we explain the data pre-processing steps for each signal type, followed by feature extraction. Next, we describe data normalization, which is followed by a description of the baseline classifiers used for benchmarking.

4.1 Pre-processing

The cognitive load scores were collected at 10-second intervals during the 3-minute driving scenarios. We segment each recording into 18 segments of 10 seconds each. These segments will later be used for feature extraction or fed directly into the deep learning models.

EEG. To remove noise and artifacts from EEG, we used a Butterworth 2nd order bandpass filter with a passband frequency of 0.4 to 75 Hz. A notch filter with a quality factor of 30, was used to remove the powerline noise at a frequency of 60 Hz.

ECG. The ECG signals experienced missing values from time to time, which we imputed using a simple 5th order polynomial interpolation technique. Artifacts such as high frequency noise, EMG noise, T noise interference, etc., were then filtered out using a butterworth bandpass filter with passband frequency of 5 to 15 Hz, which also enables us to obtain maximum QRS energy [68], [69].

EDA. For EDA there were some missing values which we replaced with a sample-and-hold strategy given the simplicity of the EDA signals (e.g., in comparison to ECG). We then used a lowpass butterworth filter with a cut-off frequency of

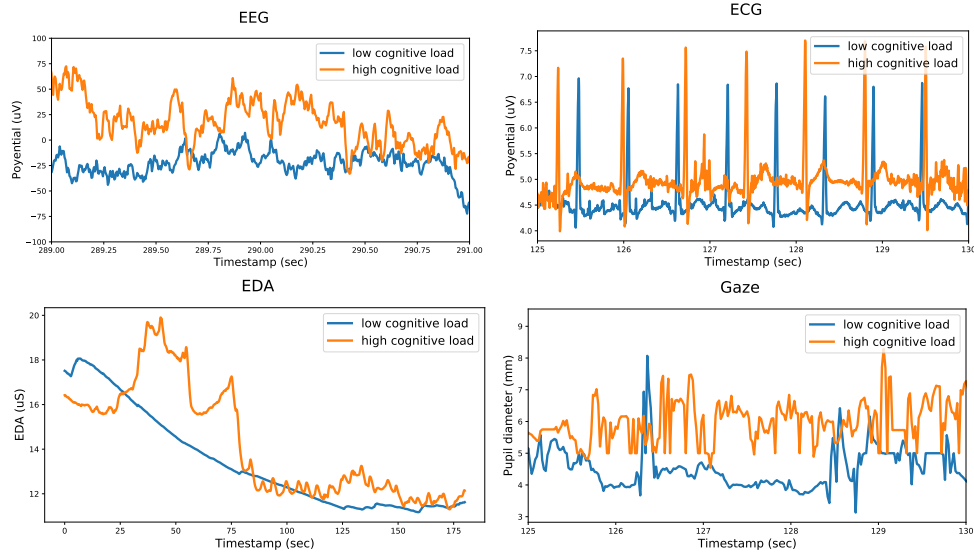


Fig. 5: Examples of different signals in high and low cognitive load scenarios.

TABLE 5: Extracted features from each modality.

Modalities	Extracted features	Number of features
EEG	PSD (absolute, mean, maximum, minimum, median power), Spectral Entropy, Hjorth mobility and complexity, Lempel-Ziv Complexity, Higuchi fractal dimension, raw signal (mean, minimum, maximum, median, variance, and standard deviation)	40
ECG	RMSSD, MeanNN, SDNN, SDDSD, CVNN, CVSD, MedianNN, MadNN, MCVNN, IQRNN, pNN50, pNN20, TINN, HTI, SD1, SD2 SD1/SD2, S, CSI, CSI_Modifies, CVI, PIP, IALS, PSS, PAS, GI, SI, AI, PI, C1d, C1a, SD1d, SD1a, C2d, C2a, SD2d, SD2a, Cd, Ca, SDNNd, SDNNA, ApEn, SampEn, mean, median, standard deviation, skewness, kurtosis, entropy, interquartile range, area under curve, squared area under the curve, median absolute deviation	53
EDA	Mean, median, standard deviation, skewness, kurtosis, entropy, interquartile range, area under curve, squared area under the curve, median absolute deviation for raw data as well as phasic and tonic response	30
Gaze	Pupil diameter (max, min, mean), Blink count, duration (max, mean), Fixation count, duration (max, min, mean), dispersion (max, min, mean), Saccade count, duration (max, min, mean), amplitude (max, min, mean), peak velocity (max, min, mean), peak acceleration (max, min, mean), peak deceleration (max, min, mean), direction (max, min, mean)	32

3 Hz to remove the unwanted noise. A highpass butterworth filter with a cut-off frequency of 0.05 Hz was used to decompose the filtered EDA signal to tonic skin conductance level and phasic skin conductance response to isolate the slow changing levels and rapid changing peaks in the signal [70].

Gaze. The device measures saccade, fixation, pupil diameter, blink count, and blink duration based on 2D gaze coordinates (x, y pixel coordinates in screen space) for both left and right eyes, 3D gaze coordinates (x, y, z coordinates in mm in camera space), 3D gaze direction (vector units), gaze velocity in degrees per second ($^{\circ}/s$), and gaze acceleration in degrees per second squared ($^{\circ}/s^2$). We directly use the high-level metrics in our study.

4.2 Feature Extraction

Different features were extracted to train our machine learning algorithms. In this section, we describe the features extracted from each modality. Please note that given the focus of our work on BCI and the EEG modality in particular (whereas other modalities play auxiliary roles in the

multimodal setups), we describe the EEG-related features in more depth below.

EEG. We extract 40 features from both time and frequency domains from each channel for each 10 seconds segment. The details of the features are given below:

- 1) **Power Spectral Density (PSD):** PSD measures the power of the EEG signal. To calculate this feature we use the Welch’s method from 0.5 Hz to 75 Hz frequency, for each frequency band, Delta (0.5-4 Hz), Theta (4-8Hz), Alpha (8-12 Hz), Beta (12-31 Hz), and Gamma (31-75 Hz). We then measure the absolute, mean, maximum, minimum, and median power of the measured PSD.
- 2) **Spectral entropy:** Spectral entropy (SE) of a time series signal is derived from normalized Shannon’s entropy [71] and can be used to determine the complexity of a signal. The formula of SE can be derived from normalized PSD or probability distribution $p(i)$ of the signal as

$$SE = \sum_{i=1}^n p(i) \ln p(i). \quad (1)$$

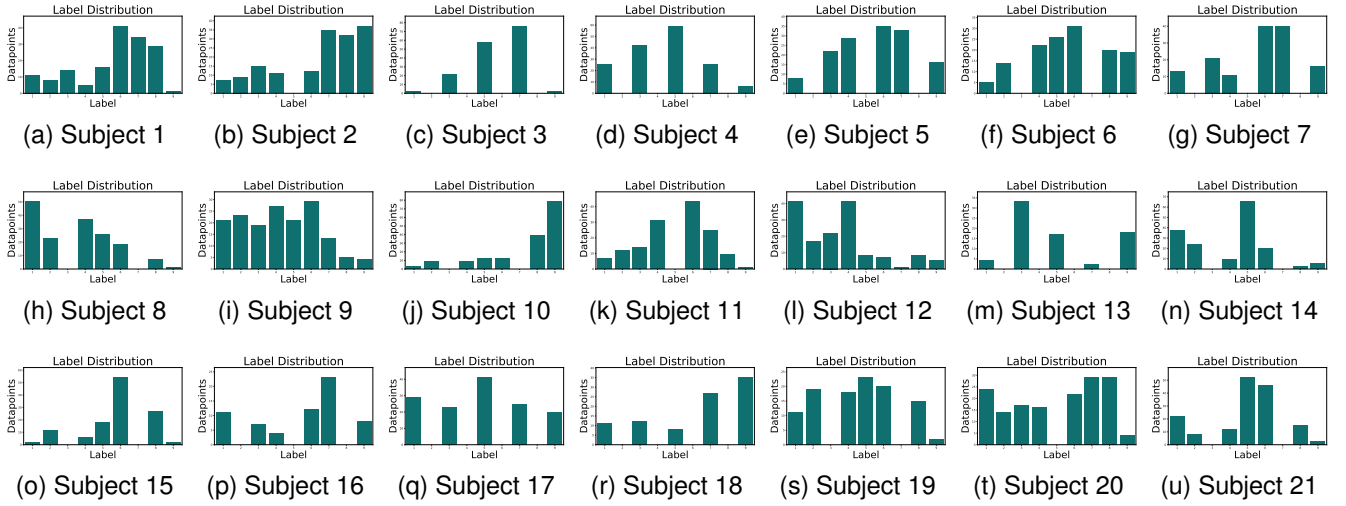


Fig. 6: Self-reported cognitive load level distribution for each participant.

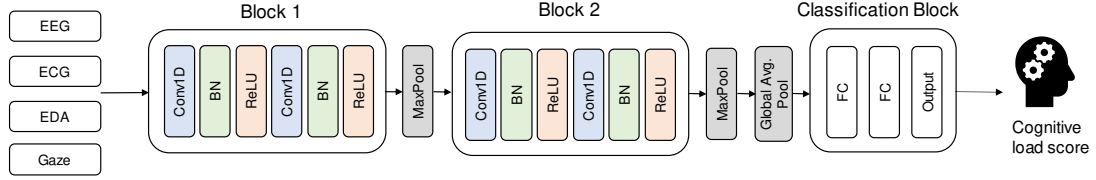


Fig. 7: VGG-style network used as for benchmarking in this study.

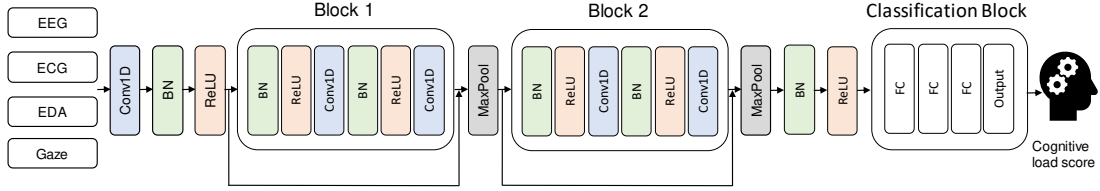


Fig. 8: ResNet-style network used as for benchmarking in this study.

- We calculate SE for all 5 bands of EEG.
- 3) **Hjorth mobility and complexity:** Both Hjorth mobility and complexity of a time series signal determine aspects of the signal complexity [72], where the variations in signal frequency and amplitude are represented by Hjorth mobility and complexity respectively. These two measurements can be jointly used to capture the dynamic behavior of signals. Hjorth mobility and complexity are respectively calculated as:

$$Hjorth_M = \sqrt{\frac{\sigma^2\left(\frac{dy(t)}{d(t)}\right)}{\sigma^2(y(t))}} \quad (2)$$

and

$$Hjorth_C = \frac{Hjorth_M\left(\frac{dy(t)}{d(t)}\right)}{Hjorth_M(y(t))}, \quad (3)$$

where $y(t)$ represents the signal and σ^2 is the variance operator.

- 4) **Lempel-Ziv complexity:** Lempel-Ziv complexity (LZC) is a measure that also determines the complexity of a signal [73]. To apply the LZC algorithm to an EEG signal, the signal first needs to be binarized by the median or mean value of the entire signal. The resulting binary sequence can then be analyzed using the LZC algorithm to find any randomness [74].
- 5) **Higuchi fractal dimension:** Higuchi fractal dimension (HFD) is a non-linear method that can capture changes in time-series signals by measuring the complexity in time domain [75]. Prior studies have shown promising results using HFD with EEG signal in the past [76], [77].
- 6) **Statistical features:** In addition to the more sophisticated features mentioned above, we also extract simple statistical features namely mean, minimum, maximum, and median from the signal in time domain.

The complete list of EEG features is summarized in Table 5. **ECCG.** We extract various commonly used features from ECCG [78]. These include both RR-based features (i.e., based on the time between two successive R-waves), HRV-based, and general statistical features. Examples include the popular pNN50 (proportion of RR intervals greater than 50ms, out of the total number of RR intervals), pNN20 (the proportion of RR intervals greater than 20ms, out of the total number of RR intervals), and others. The full list of features extracted from ECCG is presented in Table 5.

EDA. We extract a number of features from EDA. These include statistical features from the raw data as well as phasic and tonic responses which are calculated by decomposing the EDA signal. The complete list of features extracted from EDA is presented in Table 5.

Gaze. For gaze analysis, we extract statistical features for each 10-second segment. The details of all the features are given in Table 5.

4.3 Normalization

To reduce the variability *between subjects*, which is a common phenomenon when recording such data, we divide each feature value with its corresponding average value from the baseline. Second, to reduce the variability *within subjects*, we perform z-score normalization [79].

4.4 Classifiers

To evaluate the dataset and to experiment the efficacy of building an automated cognitive load detection system using the collected data, we train several classical machine learning and deep learning classifiers on the extracted features or raw data. In this section, we describe these models in detail.

4.4.1 Classical machine learning

We train a total of 9 machine learning classifiers namely AdaBoost (AB), Decision Tree (DT), Naive Bayes (NB), K-Nearest Neighbor (KNN), Linear Discriminant Analysis (LDA), Random Forest (RF), Support Vector Machine (SVM), Extreme Gradient Boosting (XGB), and Multi-Layer Perceptron (MLP). The details of the parameters of these classifiers are presented in Table 6.

4.4.2 Deep learning

For deep learning network we use two deep Convolutional Neural Networks (CNNs), a VGG-style network as shown in Figure 7, and a ResNet-style network which is shown in Figure 8. The VGG-style network has two main blocks where each block consist of two Conv1D layers, batch normalization, ReLU activation, and maximum pooling operation. These blocks are followed by two fully connected layers and a classification layer. Cross-entropy loss with a learning rate of 0.001 was used for training. ADAM was used as the optimizer for this network [80].

The ResNet-style network, similar to the VGG model above, consists of two blocks containing two Conv1D layers, batch normalization, and ReLU activation function in each block. The classification block contains three fully connected layer followed by an output classification layer. Similar to

TABLE 6: The machine learning model parameters used in this study.

Models	Parameters
AB	number of estimators: 70, learning rate: 0.1, algorithm: SAMME.R
DT	criterion: gini, random state: 42, maximum depth: 3, minimum samples to be at leaf node: 5
NB	variance smoothing: $1e^{-09}$
KNN	number of neighbors: 20, weights: distance, algorithm: 'auto'
LDA	solver: least squares solution
RF	maximum depth: 50, number of estimators: 1000, number of jobs: -1, random state: 42, class weight: balanced
SVM	regularization parameter: 0.1, kernel: polynomial
XGB	maximum depth: 20, number of estimators: 1000, learning rate: 0.001, use label encoder: False, subsample: 0.5, verbose eval: 200, booster: dart, number of jobs: -1, number of leaves: 50, regularization lambda: 0.0001, class weight: balanced
MLP	hidden layer sizes: (100, 50), learning rate: adaptive, maximum iteration: 1000

the VGG network, we use cross-entropy loss and train the model with ADAM optimizer. Here, a learning rate of 0.01 is used.

It should be noted that most studies on BCI and EEG in particular use extracted features to train deep learning models [81], [52], which is the approach we took with the networks described above. However, for completeness, we also train the deep networks with raw data (after pre-processing). For this purpose we design a separate encoder for each modality and use feature-level fusion. We expectedly notice that the optimum network depth used when utilizing the extracted features (2 blocks) is not sufficient when using the raw data. We therefore increase the depth by adding a third block to obtain better results. Accordingly each encoder for the raw data contains 3 blocks for both the VGG and ResNet-style models. The details of the architecture remain mostly the same. We present all the details of the deep networks in Table 7, for both VGG and ResNet-style models, when trained with features or raw signals.

4.5 Training scheme

We train all the models (classical machine learning and deep networks) in both 10-fold cross validation and the more rigorous Leave-One-Subject Out (LOSO) scheme. We also explore both binary and ternary classification of cognitive load. For binary, we group the cognitive load ratings from 1 to 4 as 'low' cognitive load and 5 to 9 as 'high' cognitive load. For ternary, we divide the cognitive load ratings into 3 groups, 1 to 3, 4 to 6, and 7 to 9 which corresponds to 'low', 'medium', and 'high' cognitive load classes respectively.

5 BENCHMARKING RESULTS

Here, we present the results of the benchmarking study for binary and ternary classification in both validation schemes.

TABLE 7: Architectural details of the VGG- and ResNet-style networks used in this study for both features and raw signals.

Modules	Parameters	VGG (feat.)	ResNet (feat.)	VGG (raw)	ResNet (raw)
Conv1D	Kernel size Filter size	- -	1×3 32	- -	1×32 64
Conv Block 1	Architecture Activation Kernel size Filter size Dropout rate	VGG ReLU 1×3 64 -	ResNet ReLU 1×3 32 0.5	VGG ReLU 1×32 64 -	ResNet ReLU 1×32 64 0.5
Conv Block 2	Architecture Activation Kernel size Filter size Dropout rate	VGG ReLU 1×3 128 -	ResNet ReLU 1×3 32 0.5	VGG ReLU 1×16 128 -	ResNet ReLU 1×16 128 0.5
Conv Block 3	Architecture Activation Kernel size Filter size Dropout rate	- - - - -	- - - - -	VGG ReLU 1×8 256 -	ResNet ReLU 1×8 256 0.5
Classification Block	Layer type Number of layers Dropout rate Activation	FC 2 0.25 ReLU	FC 3 - ReLU	FC 2 0.25 ReLU	FC 3 0.25 ReLU

TABLE 8: The accuracy and F1 scores for the classifiers in 10-fold binary setup.

Models	Modalities								Mean
	EEG	EEG,ECG	EEG,EDA	EEG,Gaze	EEG,ECG EDA	EEG,ECG Gaze	EEG,EDA Gaze	EEG,ECG EDA, Gaze	
AB	67.17 (55.37)	73.26 (68.43)	71.09 (66.53)	70.13 (61.29)	73.84 (69.85)	74.36 (69.75)	73.36 (69.07)	75.35 (71.80)	72.32 (66.51)
DT	65.31 (63.04)	72.77 (71.15)	69.61 (67.93)	68.17 (66.48)	73.02 (71.41)	73.12 (71.52)	72.39 (70.75)	73.98 (72.40)	71.05 (69.34)
NB	48.68 (46.54)	51.80 (50.48)	51.39 (49.97)	49.95 (48.22)	53.73 (52.87)	52.46 (51.35)	52.39 (51.23)	54.42 (53.65)	51.85 (50.54)
KNN	70.61 (68.49)	69.34 (67.40)	71.78 (70.16)	77.00 (74.65)	70.64 (69.16)	74.60 (71.97)	77.72 (75.46)	74.97 (72.50)	73.33 (71.22)
LDA	66.83 (62.45)	72.74 (70.65)	71.19 (68.45)	69.65 (66.24)	74.73 (72.94)	73.70 (71.61)	72.95 (70.62)	75.83 (74.04)	72.20 (69.63)
RF	77.41 (73.39)	79.34 (76.27)	79.48 (76.47)	79.89 (76.31)	81.26 (78.8)	80.82 (77.94)	80.65 (77.83)	81.71 (79.23)	80.07 (77.03)
SVM	61.88 (38.29)	62.08 (38.89)	61.88 (38.29)	63.46 (43.86)	64.35 (46.59)	71.54 (65.23)	67.14 (54.32)	73.70 (68.98)	65.75 (49.31)
XGB	77.38 (73.72)	82.95 (81.25)	80.06 (77.67)	80.75 (78.06)	82.61 (80.94)	83.02 (81.22)	82.12 (80.08)	83.67 (82.05)	81.57 (79.37)
MLP	74.32 (72.36)	74.22 (72.31)	76.31 (74.02)	75.18 (73.46)	76.00 (74.54)	75.83 (74.55)	77.11 (75.47)	77.69 (76.19)	75.83 (74.11)
VGG (feat.)	75.56 (73.21)	77.57 (75.8)	78.99 (76.94)	78.78 (76.74)	78.78 (77.22)	78.82 (77.23)	80.17 (78.39)	80.66 (79.17)	78.67 (68.31)
ResNet (feat.)	69.38 (65.26)	74.27 (71.48)	71.74 (68.46)	72.85 (69.15)	75.49 (72.71)	74.65 (71.83)	73.61 (70.67)	76.39 (74.28)	73.55 (70.48)
VGG (raw)	63.83 (63.23)	67.73 (66.97)	66.95 (66.11)	67.62 (66.95)	70.12 (69.2)	71.45 (70.5)	71.76 (71.07)	73.87 (73.00)	69.17 (68.38)
ResNet (raw)	61.95 (59.75)	64.49 (62.14)	60.90 (57.45)	66.68 (64.85)	64.41 (62.82)	70.04 (67.69)	68.71 (66.37)	69.96 (67.04)	65.89 (63.51)
Mean	67.72 (62.70)	70.97 (61.92)	70.11 (66.03)	70.78 (66.64)	72.23 (58.91)	73.42 (70.95)	73.08 (70.10)	74.78 (72.64)	

We also present a comparison for the different multimodal setups in our experiments. The detailed results are presented in Tables 8, 9, 10, and 11. In these tables, bold values denote the highest, while underline represents the second-highest. As we observe in Table 8, for 10-fold cross-validation in the binary setup, we obtain the highest accuracy of 83.67% with the XGB classifier. This performance is achieved when all 4 modalities are used. This is followed by 83.02% as the second best obtained with EEG with ECG and Gaze by the same classifier. Comparing the average values obtained for different modality setups indicates that as expected, EEG, ECG, EDA, and Gaze altogether outperform the rest, followed by tri-modal, bi-modal, and uni-modal setups, respectively. Looking at the average values for all the models we observe that the XGB classifier generally outperforms the rest followed by RF. Among the 4 different deep learning variants in this setup, we notice that VGG trained with features from all 4 modalities outperforms the other 3 scenarios.

In Table 9, for the binary LOSO evaluation scheme, we observe that the highest accuracy of 76.17% is obtained by the VGG-style network trained with features. This accuracy is obtained using 3 modalities, namely EEG, ECG and EDA. The second best accuracy, 76.04%, is achieved with the combination of EEG, ECG, and Gaze. Comparing the

average values from different modality setups, we observe that the highest accuracy is obtained by the multimodal scenario with all 4 modalities, followed by the tri-modal, bi-modal, and uni-modal setups respectively. From the average values for each model, we can deduce that the VGG-style model trained on features performs the best, followed by the ResNet-style model trained on features.

We present the results for the ternary 10-fold setup in Table 10, and we observe that the best result of 74.08% is achieved with the machine learning classifier, XGB. This result is obtained when EEG is trained along with all 3 auxiliary modalities. The second best accuracy of 73.60% is obtained with the same classifier when EEG, EDA, and Gaze are used together. Comparing the average results for each modality setup, we find that as expected, the using all 4 modalities outperforms the rest while the best performing average result is achieved by the XGB classifier. Among the 4 deep learning models, the VGG-style model outperforms the other 3 when trained with features. Here, the highest accuracy of 67.12% is obtained when trained with 3 modalities EEG, EDA, and Gaze.

Lastly, Table 11 shows us the result in the LOSO ternary setup. The highest result obtained is 64.53% when using the ResNet-style network trained with the raw data with 3 modalities namely EEG, ECG, and Gaze. Following, the

TABLE 9: The accuracy and F1 scores for the classifiers in LOSO binary setup.

Models	Modalities								Mean
	EEG	EEG,ECG	EEG,EDA	EEG,Gaze	EEG,ECG EDA	EEG,ECG Gaze	EEG,EDA Gaze	EEG,ECG EDA, Gaze	
AB	62.30 (46.81)	66.58 (59.47)	63.01 (54.57)	64.81 (53.53)	67.86 (62.22)	66.80 (60.05)	66.92 (59.68)	69.14 (63.60)	65.93 (57.49)
DT	54.63 (49.73)	60.33 (54.82)	57.94 (53.07)	57.57 (53.77)	60.97 (56.91)	62.13 (57.25)	61.19 (56.73)	62.00 (57.02)	59.60 (54.91)
NB	47.80 (43.54)	48.94 (45.80)	48.16 (44.71)	49.00 (45.06)	49.85 (47.52)	49.85 (47.11)	49.15 (45.71)	50.35 (48.06)	49.14 (45.94)
KNN	58.21 (53.11)	61.45 (58.09)	60.83 (56.10)	66.03 (61.42)	62.51 (59.51)	65.55 (61.10)	67.06 (62.48)	65.60 (61.36)	63.40 (59.15)
LDA	57.06 (49.61)	59.87 (55.67)	62.95 (56.99)	60.45 (54.25)	63.15 (58.60)	61.88 (57.75)	64.45 (58.97)	64.73 (60.26)	61.82 (56.51)
RF	63.82 (50.97)	65.76 (56.84)	66.64 (56.73)	65.79 (54.20)	67.95 (59.92)	66.50 (57.90)	68.94 (60.48)	70.15 (62.39)	66.94 (57.43)
SVM	62.01 (37.65)	59.85 (37.84)	61.80 (37.91)	62.56 (42.96)	61.48 (45.71)	66.26 (59.40)	65.94 (51.89)	68.53 (62.79)	63.55 (47.02)
XGB	62.98 (52.34)	66.61 (60.53)	66.39 (59.34)	66.67 (59.96)	69.37 (64.01)	68.81 (63.20)	69.73 (64.01)	71.48 (66.07)	67.76 (61.18)
MLP	57.86 (51.98)	63.64 (57.90)	63.44 (58.13)	61.45 (57.43)	64.48 (60.33)	61.32 (57.15)	65.72 (60.94)	64.51 (59.41)	62.80 (57.91)
VGG (feat.)	70.70 (64.22)	74.72 (70.68)	73.01 (68.08)	74.68 (69.91)	76.17 (71.72)	76.04 (71.83)	75.49 (71.34)	75.52 (72.44)	74.54 (70.03)
ResNet (feat.)	67.45 (61.39)	75.90 (71.62)	72.20 (66.48)	72.85 (67.53)	74.23 (69.28)	74.42 (70.32)	74.89 (69.49)	74.59 (69.55)	73.32 (68.21)
VGG (raw)	65.00 (58.92)	63.67 (57.59)	67.18 (60.78)	65.37 (59.81)	67.37 (60.84)	64.97 (58.51)	66.47 (61.79)	67.18 (61.37)	65.90 (59.95)
ResNet (raw)	65.79 (57.58)	63.99 (56.73)	69.03 (61.67)	68.03 (61.12)	68.74 (61.88)	66.67 (59.63)	66.50 (62.16)	67.69 (61.88)	67.06 (60.33)
Mean	61.20 (52.14)	63.95 (57.20)	64.04 (56.50)	64.25 (57.00)	65.70 (59.88)	65.48 (60.09)	66.34 (60.44)	67.04 (62.02)	

TABLE 10: The accuracy and F1 scores for the classifiers in 10-fold ternary setup.

Models	Modalities								Mean
	EEG	EEG,ECG	EEG,EDA	EEG,Gaze	EEG,ECG EDA	EEG,ECG Gaze	EEG,EDA Gaze	EEG,ECG EDA, Gaze	
AB	46.20 (38.35)	51.84 (48.65)	51.56 (48.78)	50.12 (44.48)	53.52 (51.62)	54.66 (51.69)	52.56 (49.66)	55.31 (53.15)	51.97 (48.30)
DT	48.95 (48.77)	56.03 (56.08)	52.08 (51.85)	52.70 (52.26)	57.48 (57.36)	58.82 (58.88)	56.14 (55.85)	58.13 (58.16)	55.04 (54.90)
NB	34.93 (29.77)	37.13 (33.00)	37.47 (33.77)	36.58 (31.86)	39.50 (36.55)	38.78 (35.06)	38.64 (35.23)	40.50 (37.74)	37.94 (34.12)
KNN	54.59 (53.95)	51.60 (50.81)	56.34 (55.90)	62.22 (62.01)	52.46 (51.67)	57.06 (56.33)	63.05 (62.87)	58.61 (57.93)	56.99 (56.43)
LDA	53.01 (51.93)	58.27 (58.09)	58.13 (57.82)	54.93 (54.33)	61.02 (61.00)	59.43 (59.23)	58.03 (57.89)	61.84 (61.84)	58.08 (57.77)
RF	63.56 (63.04)	68.41 (68.42)	69.34 (69.17)	68.30 (68.03)	71.57 (71.63)	70.40 (70.39)	71.67 (71.76)	72.67 (72.86)	69.49 (69.41)
SVM	41.01 (21.66)	46.58 (37.78)	41.73 (24.17)	48.75 (42.59)	48.40 (41.25)	53.01 (50.34)	50.39 (45.38)	53.83 (51.60)	47.96 (39.35)
XGB	64.49 (64.14)	70.78 (71.01)	71.74 (71.69)	71.19 (71.22)	73.50 (73.76)	72.91 (73.15)	73.60 (73.61)	74.08 (74.26)	71.54 (71.61)
MLP	58.44 (57.72)	61.50 (60.64)	61.12 (60.90)	62.63 (62.22)	62.80 (62.66)	63.08 (63.09)	63.84 (63.83)	63.25 (63.26)	62.08 (61.79)
VGG (feat.)	62.12 (60.92)	62.85 (62.21)	64.44 (63.91)	65.38 (64.88)	65.76 (65.37)	64.03 (63.43)	67.12 (66.72)	66.67 (66.04)	64.80 (64.19)
ResNet (feat.)	47.19 (44.61)	55.52 (53.74)	51.91 (50.66)	51.39 (49.41)	56.15 (55.48)	54.86 (53.88)	53.19 (52.24)	55.63 (54.67)	53.23 (51.84)
VGG (raw)	47.85 (43.7)	55.43 (51.37)	56.48 (51.61)	56.68 (52.24)	61.76 (57.96)	62.89 (58.3)	63.44 (59.41)	66.33 (62.93)	58.86 (54.69)
ResNet (raw)	50.82 (37.41)	56.56 (50.09)	53.67 (44.25)	56.37 (49.93)	60.62 (54.07)	59.38 (54.49)	61.05 (56.39)	64.84 (60.60)	57.91 (50.90)
Mean	51.78 (47.38)	56.35 (53.99)	55.85 (52.65)	56.71 (54.27)	58.81 (56.95)	59.18 (57.56)	59.44 (57.76)	60.90 (59.62)	

TABLE 11: The accuracy and F1 scores for the classifiers in LOSO ternary setup.

Models	Modalities								Mean
	EEG	EEG,ECG	EEG,EDA	EEG,Gaze	EEG,ECG EDA	EEG,ECG Gaze	EEG,EDA Gaze	EEG,ECG EDA, Gaze	
AB	37.79 (27.09)	42.13 (34.39)	42.56 (36.04)	43.88 (36.63)	44.26 (38.46)	45.42 (37.95)	46.03 (39.76)	47.65 (41.81)	43.15 (35.76)
DT	35.83 (33.35)	40.15 (37.63)	37.37 (34.68)	37.69 (34.8)	35.77 (33.02)	40.32 (37.76)	37.58 (35.42)	39.15 (37.17)	37.82 (35.24)
NB	33.28 (26.3)	33.81 (27.37)	33.02 (27.85)	34.27 (28.04)	33.23 (28.40)	34.71 (28.59)	33.93 (29.18)	34.08 (29.40)	33.75 (27.96)
KNN	35.19 (32.87)	39.19 (37.06)	37.40 (34.97)	44.03 (41.90)	39.24 (37.31)	41.51 (39.82)	44.78 (42.45)	41.69 (40.04)	40.19 (38.05)
LDA	36.18 (33.64)	40.23 (37.02)	40.33 (37.61)	38.43 (36.29)	42.31 (39.07)	40.02 (37.22)	40.96 (38.78)	41.03 (38.45)	39.78 (37.09)
RF	37.02 (32.58)	40.15 (37.54)	39.97 (36.05)	43.03 (39.93)	42.28 (40.15)	43.11 (40.13)	45.31 (42.38)	44.96 (42.76)	41.55 (38.39)
SVM	38.48 (20.41)	39.66 (31.73)	38.42 (21.00)	42.46 (34.15)	39.83 (33.22)	44.69 (40.43)	43.13 (35.87)	45.05 (41.22)	40.95 (30.97)
XGB	36.09 (32.83)	40.06 (38.11)	41.63 (38.50)	43.26 (41.51)	44.48 (42.31)	43.44 (40.82)	46.14 (43.77)	47.10 (44.68)	42.16 (39.69)
MLP	38.30 (34.11)	39.30 (36.70)	41.44 (36.83)	44.23 (41.10)	42.04 (38.88)	41.68 (38.99)	46.05 (42.65)	42.94 (40.38)	41.86 (38.47)
VGG (feat.)	49.21 (43.75)	54.34 (48.93)	51.83 (47.64)	54.67 (49.85)	54.39 (50.96)	53.64 (49.99)	56.16 (52.17)	56.88 (52.98)	53.46 (49.04)
ResNet (feat.)	47.30 (42.08)	52.82 (49.44)	53.44 (47.1)	50.23 (46.15)	55.31 (50.65)	53.81 (49.49)	53.26 (49.16)	55.70 (51.02)	52.31 (47.72)
VGG (raw)	57.91 (44.12)	60.84 (47.61)	58.86 (44.83)	58.08 (44.08)	61.29 (49.18)	63.04 (49.47)	57.01 (45.06)	63.56 (49.39)	59.58 (46.34)
ResNet (raw)	58.13 (42.54)	60.86 (47.30)	58.22 (43.81)	60.37 (45.90)	60.12 (46.68)	64.53 (51.40)	58.65 (46.27)	61.55 (49.93)	60.13 (46.27)
Mean	41.59 (34.28)	44.89 (39.29)	44.19 (37.45)	45.74 (40.03)	45.73 (40.64)	46.92 (41.70)	46.85 (41.76)	47.80 (43.02)	

second highest accuracy of 63.56% is obtained by the VGG-style network trained on raw data from all 4 modalities. The average results of various modality setups show that the multimodal setup with all 4 modalities achieves the highest accuracy. The average highest accuracy is obtained using the ResNet-style model followed by the VGG-style model both when trained with raw data.

In the end, to summarize our findings above, we observe that both classical machine learning and deep learning models possess the ability to distinguish between different levels of driver cognitive loads. As expected, we find that ternary classification is more challenging than binary, while LOSO on the other hand proves more difficult than 10-fold. In terms of modalities, multimodal setups generally provide more information regarding driver cognitive load, with

EEG, ECG, EDA and Gaze showing the best performances.

6 CONCLUSION

In this paper, we presented CL-Drive, a new multimodal cognitive load dataset collected during simulated driving. Our dataset, contains EEG, ECG, EDA, and Gaze data from 21 participants in a variety of different driving conditions. Subjective self-reported cognitive load scores were recorded at 10-second intervals throughout the experiment, making it a very rich and dense dataset in terms of both modalities and labels. We also provided benchmarks by evaluating our dataset in both binary and ternary label distributions for both LOSO as well as k-fold evaluation schemes.

7 ACKNOWLEDGEMENT

We would like to thank the Innovation for Defence Excellence and Security (IDEaS) program under the Department of National Defence (DND) for funding this project.

REFERENCES

- [1] M. Miyaji, H. Kawanaka, and K. Oguri, "Driver's cognitive distraction detection using physiological features by the adaboost," in *12th International IEEE Conference on Intelligent Transportation Systems*. IEEE, 2009, pp. 1–6.
- [2] O. Palinko, A. L. Kun, A. Shyrovkov, and P. Heeman, "Estimating cognitive load using remote eye tracking in a driving simulator," in *Proceedings of the Symposium on Eye-tracking Research & Applications*, 2010, pp. 141–144.
- [3] L. Fridman, B. Reimer, B. Mehler, and W. T. Freeman, "Cognitive load estimation in the wild," in *Proceedings of the Chi Conference on Human Factors in Computing Systems*, 2018, pp. 1–9.
- [4] A. Yüce, H. Gao, G. L. Cuendet, and J.-P. Thiran, "Action units and their cross-correlations for prediction of cognitive load during driving," *IEEE Transactions on Affective Computing*, vol. 8, no. 2, pp. 161–175, 2016.
- [5] J. Sweller, "Cognitive load theory," in *Psychology of Learning and Motivation*. Elsevier, 2011, vol. 55, pp. 37–76.
- [6] R. Das, D. Chatterjee, D. Das, A. Sinharay, and A. Sinha, "Cognitive load measurement—a methodology to compare low cost commercial eeg devices," in *International Conference on Advances in Computing, Communications and Informatics*. IEEE, 2014, pp. 1188–1194.
- [7] S. Schneegass, B. Pflöging, N. Broy, F. Heinrich, and A. Schmidt, "A data set of real world driving to assess driver workload," in *Proceedings of the 5th International Conference on Automotive User Interfaces and Interactive Vehicular Applications*, 2013, pp. 150–157.
- [8] I. Mijić, M. Šarlija, and D. Petrinović, "Mmod-cog: A database for multimodal cognitive load classification," in *11th International Symposium on Image and Signal Processing and Analysis*. IEEE, 2019, pp. 15–20.
- [9] V. Markova, T. Ganchev, and K. Kalinkov, "Clas: A database for cognitive load, affect and stress recognition," in *International Conference on Biomedical Innovations and Applications*. IEEE, 2019, pp. 1–4.
- [10] M. Gjoreski, T. Kolenik, T. Knez, M. Luštrek, M. Gams, H. Gjoreski, and V. Pejović, "Datasets for cognitive load inference using wearable sensors and psychological traits," *Applied Sciences*, vol. 10, no. 11, p. 3843, 2020.
- [11] A. Kalatzis, A. Teotia, V. G. Prabhu, and L. Stanley, "A database for cognitive workload classification using electrocardiogram and respiration signal," in *International Conference on Applied Human Factors and Ergonomics*. Springer, 2021, pp. 509–516.
- [12] P. Sarkar, K. Ross, A. J. Ruberto, D. Rodenburg, P. Hungler, and A. Etemad, "Classification of cognitive load and expertise for adaptive simulation using deep multitask learning," in *8th International Conference on Affective Computing and Intelligent Interaction*. IEEE, 2019, pp. 1–7.
- [13] K. Ross, P. Sarkar, D. Rodenburg, A. Ruberto, P. Hungler, A. Szulewski, D. Howes, and A. Etemad, "Toward dynamically adaptive simulation: Multimodal classification of user expertise using wearable devices," *Journal of Sensors*, vol. 19, no. 19, p. 4270, 2019.
- [14] R. Brunken, J. L. Plass, and D. Leutner, "Direct measurement of cognitive load in multimedia learning," *Educational Psychologist*, vol. 38, no. 1, pp. 53–61, 2003.
- [15] R. E. Mayer and R. Moreno, "Aids to computer-based multimedia learning," *Learning and Instruction*, vol. 12, no. 1, pp. 107–119, 2002.
- [16] M. Klepsch, F. Schmitz, and T. Seufert, "Development and validation of two instruments measuring intrinsic, extraneous, and germane cognitive load," *Frontiers in Psychology*, vol. 8, p. 1997, 2017.
- [17] F. G. Paas, "Training strategies for attaining transfer of problem-solving skill in statistics: a cognitive-load approach," *Journal of Educational Psychology*, vol. 84, no. 4, p. 429, 1992.
- [18] S. G. Hart and L. E. Staveland, "Development of nasa-tlx (task load index): Results of empirical and theoretical research," in *Advances in Psychology*. Elsevier, 1988, vol. 52, pp. 139–183.
- [19] R. Brünken, S. Steinbacher, J. L. Plass, and D. Leutner, "Assessment of cognitive load in multimedia learning using dual-task methodology," *Experimental Psychology*, vol. 49, no. 2, p. 109, 2002.
- [20] B. Park and R. Brünken, "The rhythm method: A new method for measuring cognitive load—an experimental dual-task study," *Applied Cognitive Psychology*, vol. 29, no. 2, pp. 232–243, 2015.
- [21] P. W. Van Gerven, F. Paas, J. J. Van Merriënboer, and H. G. Schmidt, "Memory load and the cognitive pupillary response in aging," *Psychophysiology*, vol. 41, no. 2, pp. 167–174, 2004.
- [22] S. Chen and J. Epps, "Using task-induced pupil diameter and blink rate to infer cognitive load," *Human-Computer Interaction*, vol. 29, no. 4, pp. 390–413, 2014.
- [23] F. G. Paas and J. J. Van Merriënboer, "Variability of worked examples and transfer of geometrical problem-solving skills: A cognitive-load approach," *Journal of Educational Psychology*, vol. 86, no. 1, p. 122, 1994.
- [24] P. Antonenko, F. Paas, R. Grabner, and T. Van Gog, "Using electroencephalography to measure cognitive load," *Educational Psychology Review*, vol. 22, no. 4, pp. 425–438, 2010.
- [25] S. Chisholm, J. K. Caird, and J. Lockhart, "The effects of practice with mp3 players on driving performance," *Accident Analysis & Prevention*, vol. 40, no. 2, pp. 704–713, 2008.
- [26] D. He, B. Donmez, C. C. Liu, and K. N. Plataniotis, "High cognitive load assessment in drivers through wireless electroencephalography and the validation of a modified n-back task," *IEEE Transactions on Human-Machine Systems*, vol. 49, no. 4, pp. 362–371, 2019.
- [27] S. Barua, M. U. Ahmed, and S. Begum, "Classifying drivers' cognitive load using eeg signals," in *pHealth*, 2017, pp. 99–106.
- [28] B. Mehler, B. Reimer, J. F. Coughlin, and J. A. Dusek, "Impact of incremental increases in cognitive workload on physiological arousal and performance in young adult drivers," *Transportation Research Record*, vol. 2138, no. 1, pp. 6–12, 2009.
- [29] B. Mehler, B. Reimer, and J. F. Coughlin, "Sensitivity of physiological measures for detecting systematic variations in cognitive demand from a working memory task: an on-road study across three age groups," *Human Factors*, vol. 54, no. 3, pp. 396–412, 2012.
- [30] J. L. Kolodner, "An introduction to case-based reasoning," *Artificial Intelligence Review*, vol. 6, no. 1, pp. 3–34, 1992.
- [31] M. Braun, J. Schubert, B. Pflöging, and F. Alt, "Improving driver emotions with affective strategies," *Multimodal Technologies and Interaction*, vol. 3, no. 1, p. 21, 2019.
- [32] C. Nass, I.-M. Jonsson, H. Harris, B. Reaves, J. Endo, S. Brave, and L. Takayama, "Improving automotive safety by pairing driver emotion and car voice emotion," in *CHI'05 Extended Abstracts on Human Factors in Computing Systems*, 2005, pp. 1973–1976.
- [33] S. Zepf, J. Hernandez, A. Schmitt, W. Minker, and R. W. Picard, "Driver emotion recognition for intelligent vehicles: A survey," *ACM Computing Surveys (CSUR)*, vol. 53, no. 3, pp. 1–30, 2020.
- [34] G. Zhang and A. Etemad, "Capsule attention for multimodal eeg-eog representation learning with application to driver vigilance estimation," *IEEE Transactions on Neural Systems and Rehabilitation Engineering*, vol. 29, pp. 1138–1149, 2021.
- [35] L. M. Bergasa, J. Nuevo, M. A. Sotelo, R. Barea, and M. E. Lopez, "Real-time system for monitoring driver vigilance," *IEEE Transactions on Intelligent Transportation Systems*, vol. 7, no. 1, pp. 63–77, 2006.
- [36] C.-T. Lin, C.-H. Chuang, C.-S. Huang, S.-F. Tsai, S.-W. Lu, Y.-H. Chen, and L.-W. Ko, "Wireless and wearable eeg system for evaluating driver vigilance," *IEEE Transactions on Biomedical Circuits and Systems*, vol. 8, no. 2, pp. 165–176, 2014.
- [37] Z. Emami and T. Chau, "The effects of visual distractors on cognitive load in a motor imagery brain-computer interface," *Behavioural Brain Research*, vol. 378, p. 112240, 2020.
- [38] W. J. Chai, A. I. Abd Hamid, and J. M. Abdullah, "Working memory from the psychological and neurosciences perspectives: a review," *Frontiers in Psychology*, vol. 9, p. 401, 2018.
- [39] S. Siuly, Y. Li, and Y. Zhang, "Eeg signal analysis and classification," *IEEE Transactions on Neural Systems and Rehabilitation Engineering*, vol. 11, pp. 141–144, 2016.
- [40] W. Klimesch, "Eeg alpha and theta oscillations reflect cognitive and memory performance: a review and analysis," *Brain Research Reviews*, vol. 29, no. 2–3, pp. 169–195, 1999.
- [41] K. Ross, P. Hungler, and A. Etemad, "Unsupervised multi-modal representation learning for affective computing with multi-corpus wearable data," *Journal of Ambient Intelligence and Humanized Computing*, pp. 1–26, 2021.

- [42] R. Xiong, F. Kong, X. Yang, G. Liu, and W. Wen, "Pattern recognition of cognitive load using eeg and ecg signals," *Journal of Sensors*, vol. 20, no. 18, p. 5122, 2020.
- [43] A. M. Hughes, G. M. Hancock, S. L. Marlow, K. Stowers, and E. Salas, "Cardiac measures of cognitive workload: a meta-analysis," *Human Factors*, vol. 61, no. 3, pp. 393–414, 2019.
- [44] E. Johannessen, A. Szulewski, N. Radulovic, M. White, H. Braund, D. Howes, D. Rodenburg, and C. Davies, "Psychophysiologic measures of cognitive load in physician team leaders during trauma resuscitation," *Computers in Human Behavior*, vol. 111, p. 106393, 2020.
- [45] J. Zagermann, U. Pfeil, and H. Reiterer, "Measuring cognitive load using eye tracking technology in visual computing," in *Proceedings of the 6th Workshop on Beyond Time and Errors on Novel Evaluation Methods for Visualization*, 2016, pp. 78–85.
- [46] S. T. Iqbal, P. D. Adamczyk, X. S. Zheng, and B. P. Bailey, "Understanding changes in mental workload during task execution," Tech. Rep., 2004.
- [47] J. Engström, G. Markkula, T. Victor, and N. Merat, "Effects of cognitive load on driving performance: The cognitive control hypothesis," *Human Factors*, vol. 59, no. 5, pp. 734–764, 2017.
- [48] P. Sena, M. d'Amore, M. Pappalardo, A. Pellegrino, A. Fiorentino, and F. Vilecco, "Studying the influence of cognitive load on driver's performances by a fuzzy analysis of lane keeping in a drive simulation," *IFAC Proceedings Volumes*, vol. 46, no. 21, pp. 151–156, 2013.
- [49] L. Cabañero, R. Hervás, I. González, J. Fontecha, T. Mondéjar, and J. Bravo, "Analysis of cognitive load using eeg when interacting with mobile devices," *Multidisciplinary Digital Publishing Institute Proceedings*, vol. 31, no. 1, p. 70, 2019.
- [50] I. Volman, K. Roelofs, S. Koch, L. Verhagen, and I. Toni, "Anterior prefrontal cortex inhibition impairs control over social emotional actions," *Current biology*, vol. 21, no. 20, pp. 1766–1770, 2011.
- [51] G. Zhang and A. Etemad, "Deep recurrent semi-supervised eeg representation learning for emotion recognition," in *9th International Conference on Affective Computing and Intelligent Interaction*. IEEE, 2021, pp. 1–8.
- [52] G. Zhang, V. Davoodnia, and A. Etemad, "Parse: Pairwise alignment of representations in semi-supervised eeg learning for emotion recognition," *IEEE Transactions on Affective Computing*, 2022.
- [53] J. R. Stroop, "Studies of interference in serial verbal reactions," *Journal of Experimental Psychology*, vol. 18, no. 6, p. 643, 1935.
- [54] F. Schmiedek, M. Lövdén, and U. Lindenberger, "A task is a task is a task: putting complex span, n-back, and other working memory indicators in psychometric context," *Frontiers in Psychology*, vol. 5, p. 1475, 2014.
- [55] Y. Santiago-Espada, R. R. Myer, K. A. Latorella, and J. R. Comstock Jr, "The multi-attribute task battery ii (matb-ii) software for human performance and workload research: A user's guide," Tech. Rep., 2011.
- [56] A. Morley, L. Hill, and A. Kaditis, "10-20 system eeg placement," *European Respiratory Society, European Respiratory Society*, 2016.
- [57] V. Jurcak, D. Tsuzuki, and I. Dan, "10/20, 10/10, and 10/5 systems revisited: their validity as relative head-surface-based positioning systems," *Neuroimage*, vol. 34, no. 4, pp. 1600–1611, 2007.
- [58] A. Burns, B. R. Greene, M. J. McGrath, T. J. O'Shea, B. Kuris, S. M. Ayer, F. Stroiescu, and V. Cionca, "SHIMMER—a wireless sensor platform for noninvasive biomedical research," *IEEE Sensors Journal*, vol. 10, no. 9, pp. 1527–1534, 2010.
- [59] M. Rizzo, P. A. Sheffield, L. Stierman, and J. Dawson, "Demographic and driving performance factors in simulator adaptation syndrome," in *Driving Assessment Conference*, vol. 2, no. 2003. University of Iowa, 2003.
- [60] J. G. Reed-Jones, W. J. Reed-Jones, L. M. Trick, R. Toxopeus, and L. A. Vallis, "Comparing techniques to reduce simulator adaptation syndrome and improve naturalistic behaviour during simulated driving," in *Driving Assessment Conference*, vol. 5, no. 2009. University of Iowa, 2009.
- [61] T. G. Dobbie, *Motion sickness: a motion adaptation syndrome*. Springer, 2019, vol. 6.
- [62] S. V. Cobb, S. Nichols, A. Ramsey, and J. R. Wilson, "Virtual reality-induced symptoms and effects (vrise)," *Presence: Teleoperators & Virtual Environments*, vol. 8, no. 2, pp. 169–186, 1999.
- [63] G. Gálvez-García, J. Albayay, L. Rehbein, and F. Tornay, "Mitigating simulator adaptation syndrome by means of tactile stimulation," *Applied Ergonomics*, vol. 58, pp. 13–17, 2017.
- [64] L. Frank, R. S. Kennedy, R. S. Kellogg, and M. E. McCauley, "Simulator sickness: A reaction to a transformed perceptual world. 1. scope of the problem," ESSEX CORP ORLANDO FL, Tech. Rep., 1983.
- [65] R. S. Kennedy, N. E. Lane, K. S. Berbaum, and M. G. Lilienthal, "Simulator sickness questionnaire: An enhanced method for quantifying simulator sickness," *The International Journal of Aviation Psychology*, vol. 3, no. 3, pp. 203–220, 1993.
- [66] P. J. Gianaros, E. R. Muth, J. T. Mordkoff, M. E. Levine, and R. M. Stern, "A questionnaire for the assessment of the multiple dimensions of motion sickness," *Aviation, Space, and Environmental Medicine*, vol. 72, no. 2, p. 115, 2001.
- [67] F. G. Paas, "Training strategies for attaining transfer of problem-solving skill in statistics: a cognitive-load approach," *Journal of Educational Psychology*, vol. 84, no. 4, p. 429, 1992.
- [68] N. Thakor, J. Webster, and W. Tompkins, "Optimal qrs detector," *Medical and Biological Engineering and Computing*, vol. 21, no. 3, pp. 343–350, 1983.
- [69] H. G. Goovaerts, H. H. Ros, T. J. Van Den Akker, and H. Schneider, "A digital qrs detector based on the principle of contour limiting," *IEEE Transactions on Biomedical Engineering*, no. 2, pp. 154–160, 1976.
- [70] C. L. Lim, C. Rennie, R. J. Barry, H. Bahramali, I. Lazzaro, B. Manor, and E. Gordon, "Decomposing skin conductance into tonic and phasic components," *International Journal of Psychophysiology*, vol. 25, no. 2, pp. 97–109, 1997.
- [71] C. E. Shannon, "A mathematical theory of communication," *The Bell System Technical Journal*, vol. 27, no. 3, pp. 379–423, 1948.
- [72] B. Hjorth, "Eeg analysis based on time domain properties," *Electroencephalography and Clinical Neurophysiology*, vol. 29, no. 3, pp. 306–310, 1970.
- [73] A. Lempel and J. Ziv, "On the complexity of finite sequences," *IEEE Transactions on Information Theory*, vol. 22, no. 1, pp. 75–81, 1976.
- [74] F. Kaspar and H. Schuster, "Easily calculable measure for the complexity of spatiotemporal patterns," *Physical Review A*, vol. 36, no. 2, p. 842, 1987.
- [75] T. Higuchi, "Approach to an irregular time series on the basis of the fractal theory," *Physica D: Nonlinear Phenomena*, vol. 31, no. 2, pp. 277–283, 1988.
- [76] A. H. Al-Nuaimi, E. Jammeh, L. Sun, and E. Ifeachor, "Higuchi fractal dimension of the electroencephalogram as a biomarker for early detection of alzheimer's disease," in *39th Annual International Conference of the IEEE Engineering in Medicine and Biology Society*. IEEE, 2017, pp. 2320–2324.
- [77] E. Shamsi, M. A. Ahmadi-Pajouh, and T. S. Ala, "Higuchi fractal dimension: An efficient approach to detection of brain entrainment to theta binaural beats," *Biomedical Signal Processing and Control*, vol. 68, p. 102580, 2021.
- [78] F. Shaffer and J. P. Ginsberg, "An overview of heart rate variability metrics and norms," *Frontiers in Public Health*, p. 258, 2017.
- [79] P. Sarkar and A. Etemad, "Self-supervised ecg representation learning for emotion recognition," *IEEE Transactions on Affective Computing*, 2020.
- [80] D. P. Kingma and J. Ba, "Adam: A method for stochastic optimization," *International Conference on Learning Representations*, 2015.
- [81] W.-L. Zheng, W. Liu, Y. Lu, B.-L. Lu, and A. Cichocki, "Emotionmeter: A multimodal framework for recognizing human emotions," *IEEE Transactions on Cybernetics*, vol. 49, no. 3, pp. 1110–1122, 2018.